

# Quasicrystals

An-Pang Tsai

*Institute of Multidisciplinary Research for Advanced Materials, Tohoku University, Sendai 980-8577, Japan*  
*E-mail address: aptsai@tagen.tohoku.ac.jp*

(Received January 11, 2015; Accepted March 9, 2015)

Quasicrystals display diffraction patterns with symmetries forbidden in crystallography, and quasi-periodicity, have been found to be stable phases in several alloy systems. Thanks to their stability, one can grow single grained quasicrystals with large scale. In this article, we will first make a brief introduction to quasicrystals and describe the state of the art of structure for icosahedral quasicrystal. The morphologies of icosahedral quasicrystals are discussed in terms of atomic structures, surface structures and crystal growth mechanism.

**Key words:** Quasicrystal, Stable Phase, Icosahedral Cluster, Crystal Growth, Morphology

## 1. Introduction to Quasicrystal

Quasicrystal is a new form of matter, which differs from crystalline and amorphous materials by exhibiting a new ordered structure, quasiperiodicity and symmetries, such as five-fold, ten-fold, eight-fold and twelve-fold symmetries, which are forbidden in the classic crystallography. However, a diffraction pattern with five-fold symmetry, namely “quasicrystal” reported by Shechtman *et al.* (1984), has promoted a paradigm shift in understanding solid structures. Consequently, Nobel Prize in Chemistry of 2011 was awarded to Dan Shechtman for “the discovery of quasicrystal”. In this section, it is described first why and how important the quasicrystal is, then a basic concept of structure of quasicrystal is explained and finally some examples with beautiful morphologies are given. Parts of description and figures are reused from reference (Tsai and Cui, 2015).

### 1.1 Crystal and periodicity

The structures of crystals are realized with Bragg’s law, where the atoms are arranged periodically in three-dimensions. The Bragg’s law is shown in Eq. (1)

$$2d \sin \theta = n\lambda, \quad (1)$$

where  $d$  and  $\lambda$  are the lattice spacing of a crystal and the wavelength of radiation, respectively,  $\theta$  is the incident angle of radiation and  $n$  is an integer of arbitrary value. Since  $\lambda$  is fixed, diffraction is generated when  $\theta$  and  $d$  satisfy the Bragg’s law. Equation (1) can be rewritten as  $\sin \theta = n\lambda/2d$ . Here,  $d$  represents a distance between equidistance lattice planes which is inversely proportional to  $\sin \theta$ ; this formula implies that periodicity of atomic planes is required for generating diffractions.

For an example, observation of crystal was performed with a transmission electron microscopy operated with accelerating voltage at 200 kV as shown in Fig. 1(a),  $\lambda$  would have been around 0.003 nm which is much smaller than  $d$ , hence  $\sin \theta \cong \theta$ . Then, Eq. (1) could be simplified

to  $\theta = n\lambda/2d$ . Note the relationship among  $\lambda$ ,  $d$  and  $\theta$  shown in Fig. 1(a) satisfies Bragg’s law. Therefore,  $\theta$  is approximately inversely proportional to  $d$ . On the other hand, the camera constant  $L$  is the distance between the specimen and screen, where diffraction patterns are projected, and is a constant parameter of the microscopy. The length  $r$  is a distance between the transmitted peak and diffraction peaks on the screen, which is measurable from diffraction pattern. Once  $r$  is obtained, one can easily determine  $d$  or  $\theta$ . Note that  $r$  is inversely proportional to  $d$ . With this in mind, let us see a diffraction pattern generated from a square lattice as shown in Fig. 1(b).

For example, let a sequence of a lattice spacing  $d$  generate a diffraction with distance  $r = d^*$  on the diffraction pattern, then the other sequence of lattice spacing  $D (=2d)$  would generate a diffraction with  $r = D^*$ , where  $D^* = d^*/2$ . Although the diffraction is reciprocal to the corresponding lattice spacing, both of them share the same property of periodicity. That is, the arrangement of diffractions generated by a crystal with periodic structure (real lattice) must be periodic in the diffraction pattern (reciprocal lattice). In the definition of Bragg’s law, occurrence of diffractions is equivalent to periodicity and the “periodicity” is considered to be another name of crystals in classical crystallography. For a two-dimensional square lattice, the same periodic arrangement of diffractions would be observed in the two-dimensional reciprocal lattice along the vertical direction. As a result, diffractions form a square arrangement in the diffraction pattern analogous to its original lattice and a similar correlation must be observed in any three-dimensional lattice as well. An important feature inherent in this correlation is that the shape in the real lattice is preserved in the reciprocal lattice. Therefore, one would be able to recognize in Fig. 1(b) that, if the real lattice is described by repetition of a square, then one must be able to find a square to describe the reciprocal lattice. The words “repetition” and “translation” represent different meaning but they are commonly used to describe the “periodicity”. Therefore, for a long time the “periodicity” has been another name of crystal

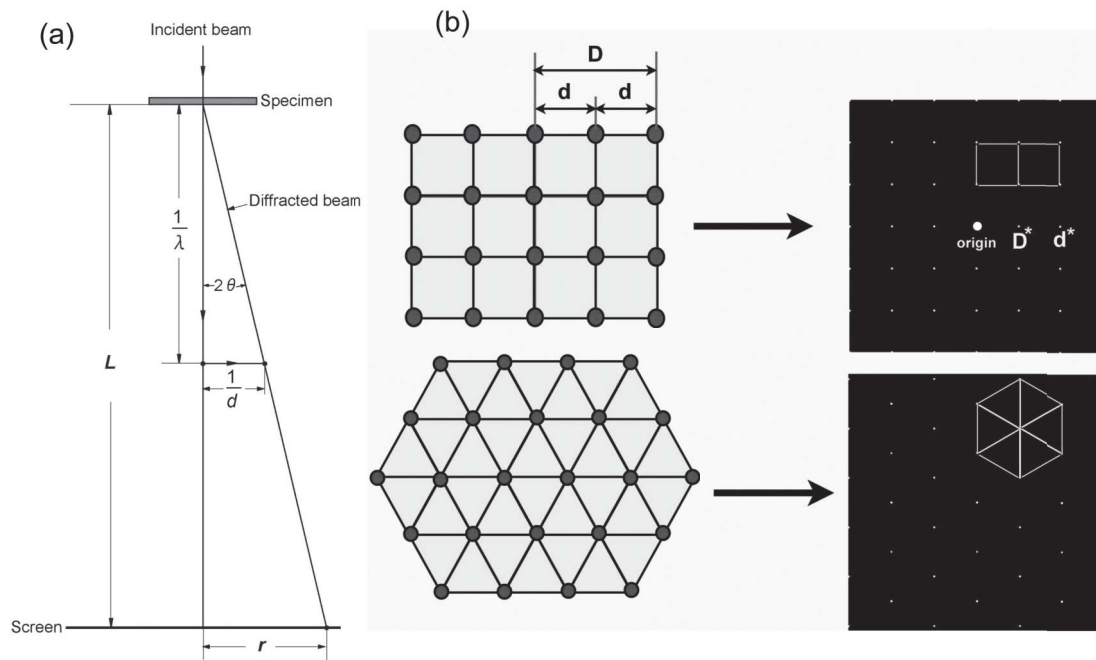


Fig. 1. (a) Schematic description of formation of diffraction pattern in transmission electron microscopy (TEM). (b) Real square and triangular lattices and their corresponding calculated diffraction patterns.

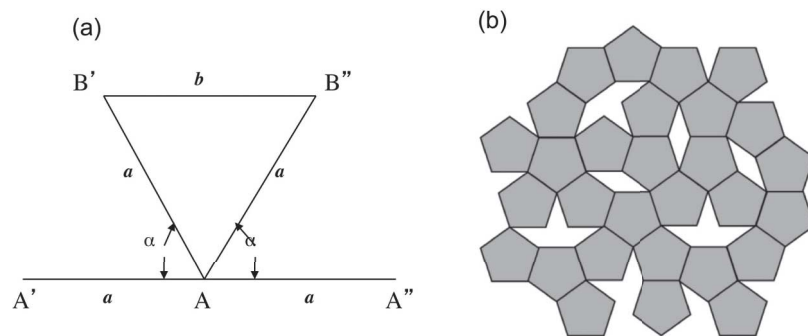


Fig. 2. Descriptions of (a) rotational symmetries compatible with lattice translation and (b) impossibility of tiling only by using pentagon.

until the discovery of QC (quasicrystal).

### 1.2 Restriction on symmetry by translation

Since a crystal structure is composed of a translation of the lattice and point group of symmetry of the basis, only a limited number of symmetries are allowed. Restriction of symmetry due to translation is described in Fig. 2(a). Consider a crystal containing lattice points of  $A, A', A'', B'$  and  $B''$ , and assume that distances from  $A$  to the other lattice points are commonly  $a$ . If angles between lines formed by lattice points are  $\alpha$ , then  $n\alpha = 360^\circ = 2\pi$ , where  $n$  is an integer which represents the order of rotational symmetry. Let  $AB = b$ , then  $b = ma$  must be satisfied with integer  $m$  in order to satisfy the translational symmetry. From a relation  $b = 2a \cos \alpha$ , we have  $\cos \alpha = m/2$ . Since  $m$  must be an integer, only a number of rotation angles are allowed as shown in Table 1. Consequently, the allowed values of  $n$  are 1, 2, 3, 4 and 6, and no any rotation symmetry with  $n > 6$  is allowed. According to this derivation, five-fold symmetry and its multiplicity are not allowed in the classical crystallography.

This can also be easily understood in terms of tiling by using a regular pentagon as shown in Fig. 2(b), where rhombus cavities would come out inevitably. In other words, a basis or a motif with five-fold symmetry does not have a possibility to fill two-dimensional plane or three-dimensional space.

### 1.3 Establishment of quasicrystal

Electron diffraction pattern obtained from the Al-Cu-Fe QC (Tsai, 2013) shown in Fig. 3(a), was in conflict with the definition and the restriction of crystal. First, as shown with guidelines, instead of periodic arrangement the arrangement of diffraction spots inflates with  $\tau$  scaling, where  $\tau$  is the golden mean ( $\approx 1.618$ ). Secondly, various sizes of pentagons formed by diffraction spots are observed on the diffraction patterns, indicating that the structure contains atomic arrangement with five-fold symmetry. Thirdly, the diffraction spots are sharp enough to deny the possibility that the quasicrystal is formed by some kinds of disorder of crystalline phases. Consequently, stable QCs, revealing sharp diffractions verified in a sequence of alloys, es-

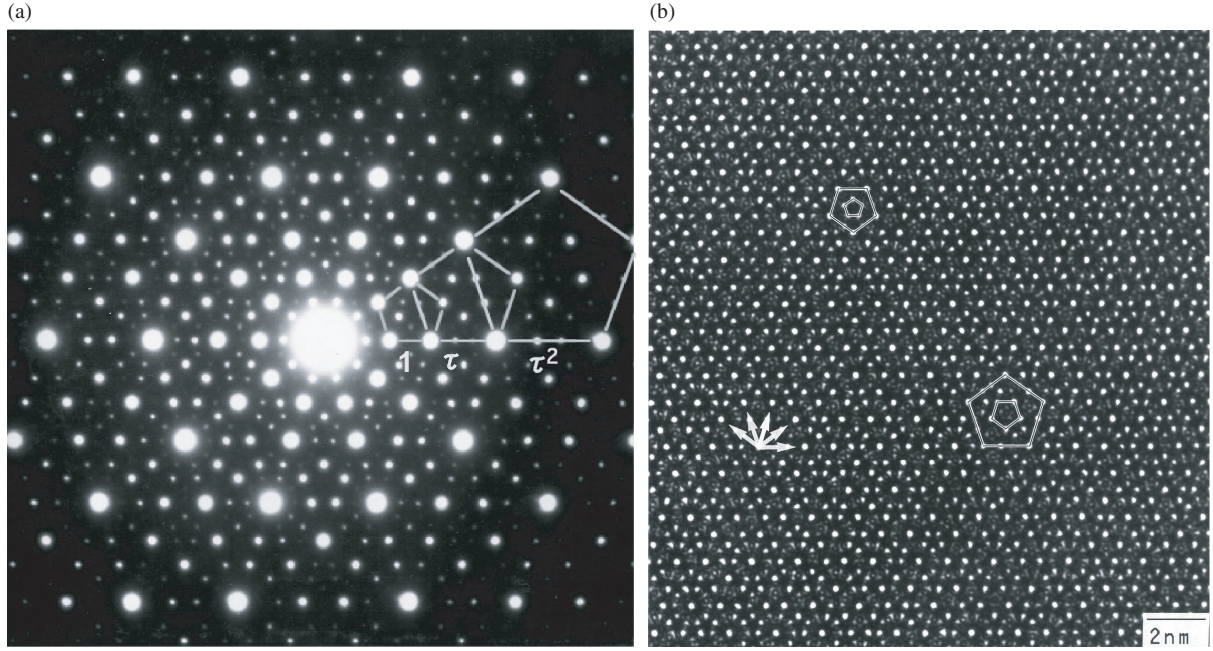


Fig. 3. (a) Electron diffraction pattern and (b) high-resolution TEM image of the stable  $\text{Al}_{65}\text{Cu}_{20}\text{Fe}_{15}$  IQC taken along a fivefold axis.

Table 1. Rotational symmetries compatible with lattice translation.

$m$	$\cos \alpha = m/2$	$\alpha$	$n = 360^\circ/\alpha$
2	1	$0, 2\pi$	1
1	$1/2$	$\pi/3$	6
0	0	$\pi/2$	4
-1	$-1/2$	$2\pi/3$	3
-2	-1	$\pi$	2

tablished that the QCs belong to a new form of solid (International Union of Crystallography, 1992). The highly ordered structure as shown in Fig. 3(b) maintained over a wide-range as large as the order of 1 mm. The International Union of Crystallography (IUCr) redefined the crystal in 1991, and the new definition of crystal is “A crystal means any solid having an essentially discrete diffraction diagram”. In the new definition the QC, as will be described later, is a crystal in high-dimensional space.

## 2. Structures of Quasicrystals

“Where are the atoms?” was put as the first question soon after the discovery of QC (International Union of Crystallography, 1992). It took few decades to establish the methodology of structural analysis for QC and to meet the available samples. Nowadays, a number of structural models with similar precisions to those of crystals are available. Here, we first describe the basic concept to understand the framework of structure of QC and then close up one real examples of structure with accurate atomic decoration.

### 2.1 One-dimensional quasi-periodic structure and Fibonacci sequence

One-dimensional quasilattice obtained by cut and projection method (de Bruijn, 1981) as shown in Fig. 4(a) is the best example to describe “how does a high-dimensional

crystal convert to a quasicrystal?” First, let us put a square lattice in two-dimensional space, and introduce a set of orthogonal axes, namely  $r^{\parallel}$  and  $r^{\perp}$ , which are rotated by an angle of  $\theta$  from the original coordinate system of the square lattice. They are called a physical and a complementary axes, respectively, and have a role to indicate the directions of projections.

Here, we introduce a strip with a width of a unit square ( $W$ ) parallel to  $r^{\parallel}$ , along  $r^{\perp}$ . This strip is called “window” for projection, which contains a number of lattice points of the square lattice. The next step is to project the lattice points inside the window on to  $r^{\parallel}$  as is shown in Fig. 4. Then, an arrangement of two different line segments with lengths  $L$  and  $S$  is obtained, as a result of the projections of two different sides of the unit square lattice. If the  $\tan \alpha$  is an irrational number, such as the case in Fig. 4(a) where  $\alpha = \tan^{-1}(1/\tau) \approx 31.716^\circ$ , a one-dimensional quasiperiodic tiling with long ( $L$ ) and short ( $S$ ) line segments is formed. Note that, if a window with smaller (larger)  $W$  is used, points of projection will be less (more) dense and  $L$  and  $S$  line segments will be larger (smaller). Note that the value of  $W$  only changes the density of projection points or the lengths of  $L$  and  $S$ , so long as the slope is the same, and one gets the same quasiperiodic array and the same length ratio,  $S/L (=1/\tau)$ . This is a property of self-similarity and the factor of self-similarity of the quasi-periodic array is irrational. If the slope of  $W$ , i.e.  $m (=S/L)$ , approaches to a rational number, for example to  $m = 2/3$  as shown in Fig. 4(b), the projection points will form a periodic array with interval of  $2S + 3L$ , which is much longer than the periodicity length of the original cubic lattice. In terms of crystallography, the quasiperiodic array is looked upon as a one-dimensional quasicrystal (Fig. 4(a)), while the periodic array derived by projection is an approximant crystal (Fig. 4(b)). By choosing continued-fractions approximant

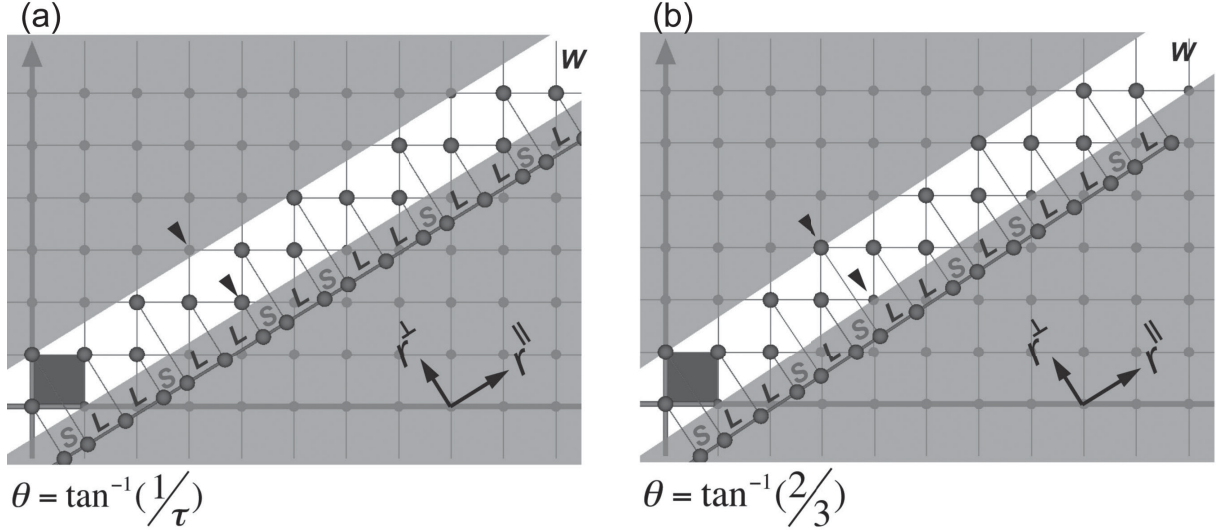


Fig. 4. Projection of a two-dimensional lattice onto a one-dimensional space with (a) an irrational slope ( $1/\tau$ ) and (b) a rational slope ( $2/3$ ) to obtain a one-dimensional QC and its approximant, respectively.

to  $\tau$  ( $m = 1/1, 1/2, 2/3, 3/5 \dots$ ) for  $m$ , one creates structures with larger periods which approximate the quasiperiodic tiling better and better, where Fig. 4(b) shows one example of the fractions. Differences between two sequences are indicated with arrowheads where  $L$ - $S$  observed in quasiperiodic tiling is replaced by  $S$ - $L$  in the approximant (Elsner and Henley, 1985). Note that a period of the approximant is made of  $LSLLS$ . The difference between the two sequences is due to a flipping between  $L$  and  $S$ , and in terms of QC this flipping is called “phason flipping” which is a sort of defect in QC. The flipping between  $L$  and  $S$  is caused by a slight change of  $m$ .

Since the one-dimensional quasi-periodic structure can be derived from two-dimensional periodic structure as shown in Fig. 4, QC is looked upon as a crystal in high-dimensional space. On the other hand, the one-dimensional quasi-periodic sequence can be obtained by a substitution rule:  $L \rightarrow LS$  and  $S \rightarrow L$ , which can be expressed as

$$\begin{pmatrix} L \\ S \end{pmatrix} \rightarrow \begin{pmatrix} 1 & 1 \\ 1 & 0 \end{pmatrix} \begin{pmatrix} L \\ S \end{pmatrix}. \quad (2)$$

If all neighboring atoms are separated by either  $L$  or  $S$  with  $L/S = \tau$ , under the substitution, a sequence of intervals is transformed to another sequence (with intervals  $\tau$  times larger than the original sequence). If we start from  $L$ , a series of sequences can be obtained, as follows:

$$\begin{aligned} &L \\ &LS \\ &LSL \\ &LSLLS \\ &LSLLSLSL \\ &LSLLSLSLLS \\ &\dots \end{aligned} \quad (3)$$

Each series in this sequence is a combination of the former two series, and can be expressed as  $F_n = F_{n-1} + F_{n-2}$ , where  $\lim_{n \rightarrow \infty} F_{n-1}/F_n = 1/\tau$ . Number of total  $L$  and

$S$  for each series will be 1, 2, 3, 5, 8, 13, 21, 34, 55, 89,  $\dots$ , which constitute the Fibonacci sequence. Note that a series of ratio of numbers such as  $1/2, 2/3, 3/5, 5/8 \dots$  are corresponding to  $m$  used to obtain a series of approximant crystals.

## 2.2 Two-dimensional quasi-periodic structure and Penrose pattern

There are a number of two-dimensional quasi-periodic structures owning different symmetries, such as eight-fold (octagonal), ten-fold (decagonal) and twelve-fold (dodecahedral) symmetries (Tsai, 1999). In reality, QCs with decagonal lattice (decagonal quasicrystal, DQC) are well studied and are stable; here we only close up the decagonal lattice. The typical decagonal lattice is described by the well-known Penrose pattern shown in Fig. 5(a). Penrose pattern is constructed by tiling two-dimensional plane tiles with two different rhombic tiles, namely a “fat” tile with an angle  $\pi/5$  and a “skinny” one with an angle  $\pi/10$ . A perfect Penrose pattern is formed only when tiling is made along the so-called “matching rules” which are formulated based on markings of the edges of tiles. Each rhombus has single or double arrows along the edges; rhombi of the same type have identical arrow markings. To make a Penrose tiling, one should fit these rhombic tiles together according to the matching rule: two rhombic tiles can be placed side by side only if fitted edges have the same type and direction of the arrows. This leads to the quasi-periodicity of tiling. Each vertex in an infinite Penrose tiling is surrounded by one of eight combinations of tiles (Henley, 1986). In the mean time, in an infinite Penrose tiling, ratio between number of fat tiles ( $N_F$ ) and that of skinny tiles ( $N_S$ ) approaches to  $\tau$ . Any vertex with surrounding tiles out of these eight combinations will be a defect, and the ratio of  $N_F/N_S$  will deviate from  $\tau$ .

Penrose pattern could be obtained by cut and projection method of a five-dimensional cubic lattice onto a two-dimensional space, similar to the case of two-dimensional

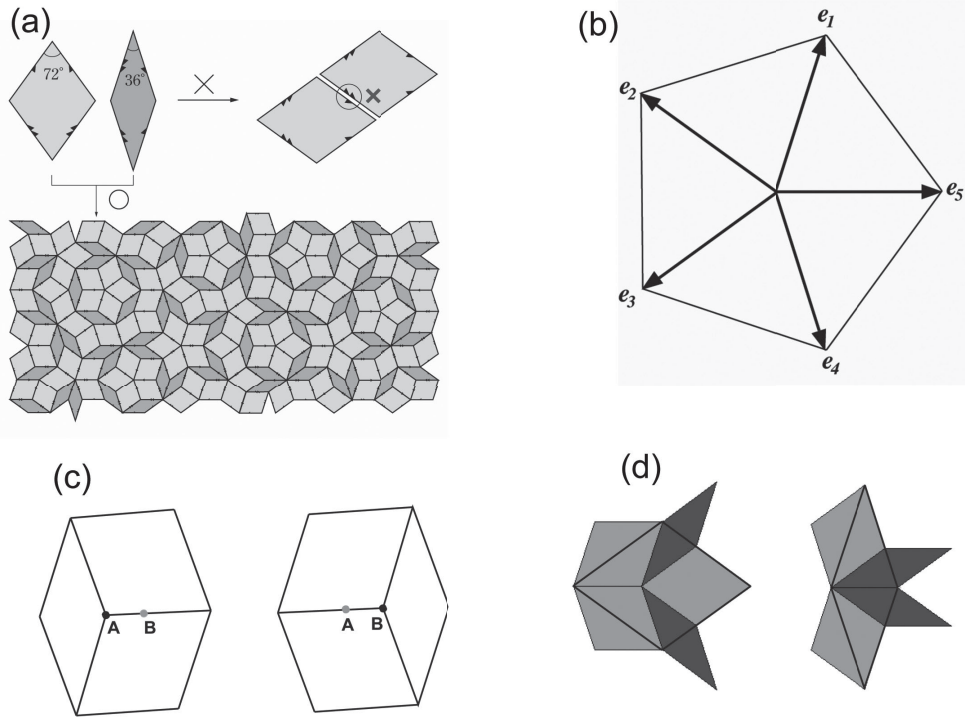


Fig. 5. (a) Description of Penrose tiling made with two rhombi, (b) five basis vectors used to index Penrose lattice, (c) description of phason flip: lattice position exchange between A and B changes the arrangement of tiles, (d) inflation in Penrose tiling.

square lattice shown in Fig. 4. In the Penrose case, instead of a strip shown in Fig. 4, a number of polygons, namely, windows of pentagons (also called occupation domains) are used. Vertex of Penrose patterns forms a two-dimensional QC, which could be assigned with five vectors,  $e_1, e_2, e_3, e_4$  and  $e_5$  as shown in Fig. 5(b) with an angle of intersection of  $\pi/5$ . Since  $e_1 + e_2 + e_3 + e_4 = -e_5$ , four vectors are enough for assignment. On the other hand, every spot in its diffraction pattern can be indexed with a combination of the vectors  $(\cos(2\pi j/5), \sin(2\pi j/5))/a$  (Yamamoto, 1996), where  $a$  is the edge length of Penrose pattern and  $j = 1, \dots, 5$ .

A typical “flipping of tiles” as shown in Fig. 5(c) is also considered as a mismatching in Penrose tiling, and this could be made through a projection with shift or a change in size of the window  $W$ . These two hexagons have the same contour and are made of two skinny and one fat tiles, but their arrangements are different. As a problem of tiling the “flipping of tiles” makes a significant difference. However, if we assume seven vertices are all occupied by atoms, this flipping is simply a slight shift of atomic position from A to B (or B to A) inside of hexagons. This is a “phason flipping” in a two-dimensional QC, which has been observed in real QC samples.

There is a self-similarity of Penrose pattern as shown in Fig. 5(d). By dividing the two edges of original tiles with length ratio of  $1 : \tau$ , one may obtain identical tiles with a scale  $1/\tau$  of the original ones. Let  $F, S, f$  and  $s$  represent the numbers of large fat, large skinny, small fat and small skinny tiles, respectively, then we have  $F = 2f + s$  and  $S = f + s$ , which can be expressed also as

$$\begin{pmatrix} F \\ S \end{pmatrix} \rightarrow \begin{pmatrix} 2 & 1 \\ 1 & 1 \end{pmatrix} \begin{pmatrix} f \\ s \end{pmatrix}. \quad (4)$$

With this relationship, we may make a deflation or an inflation operation of Penrose pattern with a scaling of  $\tau$ .

In the Penrose pattern, a large number of vertices reveal local fivefold symmetry, and there is no periodicity of lattice spacing along any direction. Calculated diffraction pattern of Penrose pattern reveals a ten-fold symmetry and a quasi-periodic arrangement of diffractions inflated with  $\tau$  scaling, which resembles very much to that observed by Shechtman *et al.* (1984). Obviously, the Penrose pattern is a key to understand structure of QC, and normally is used as a template for modeling structure of two-dimensional QC by decorating rhombic tiles with atoms. Penrose pattern itself is a decagonal structure with a ten-fold axes, and provides the simplest way to describe the DQC as a template.

### 2.3 Three-dimensional quasi-periodic structure

There is only one three-dimensional quasi-periodic structure: a QC with icosahedral symmetry or an icosahedral quasicrystal (IQC), whose electron diffraction patterns and morphology are shown in Fig. 6, which is analogical to the structure of QC observed in the Al-Mn alloy. The simplest set of unit cells for three-dimensional quasi-periodic structure consists of the acute and obtuse rhombohedra shown in Fig. 7(a). In the left (right) rhombohedron in Fig. 7(a) three vertices of rhombus with acute (obtuse) angle gather at two vertices of the rhombohedron. These two unit cells play the same roles, respectively, as the skinny and the fat tiles in the Penrose tiling. All the faces are identical rhombuses, which are the Golden rhombus with length ratio  $\tau$  of two diagonals. One can match these two cells face to face so that rhombohedra can only fill space quasi-periodically. In an infinite packing of these unit cells in three-dimension, it consists of that acute and obtuse rhom-

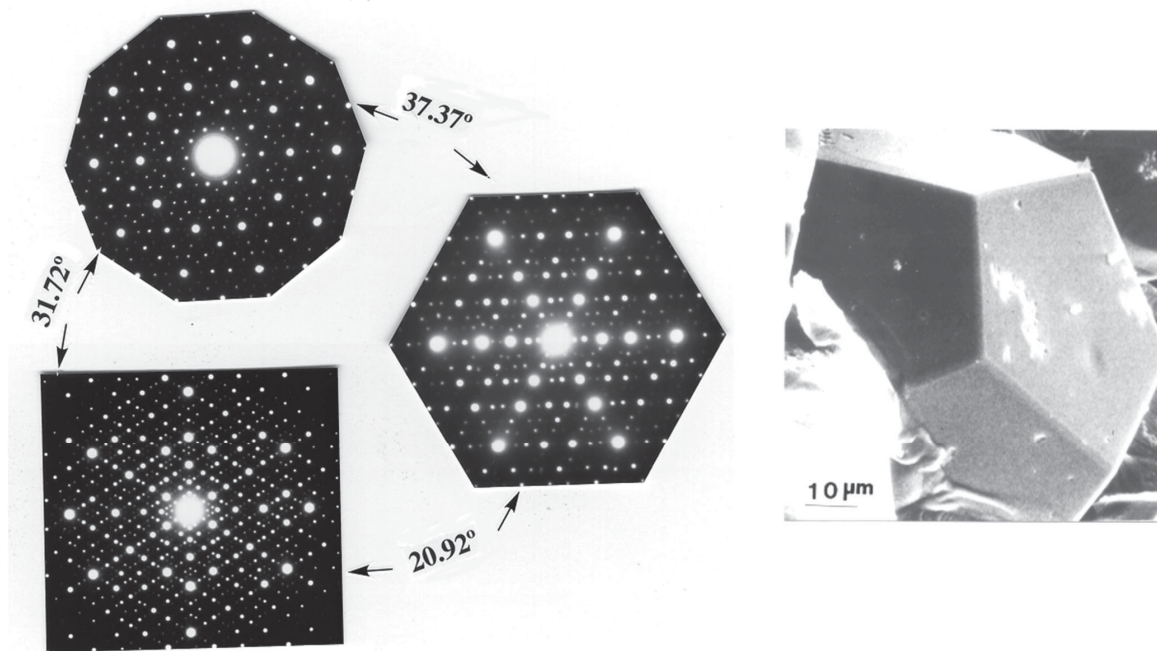


Fig. 6. Electron diffraction patterns taken along five-fold, three-fold and two-fold axes (left) and a SEM image (right) of stable  $\text{Al}_{65}\text{Cu}_{20}\text{Fe}_{15}$  IQC.

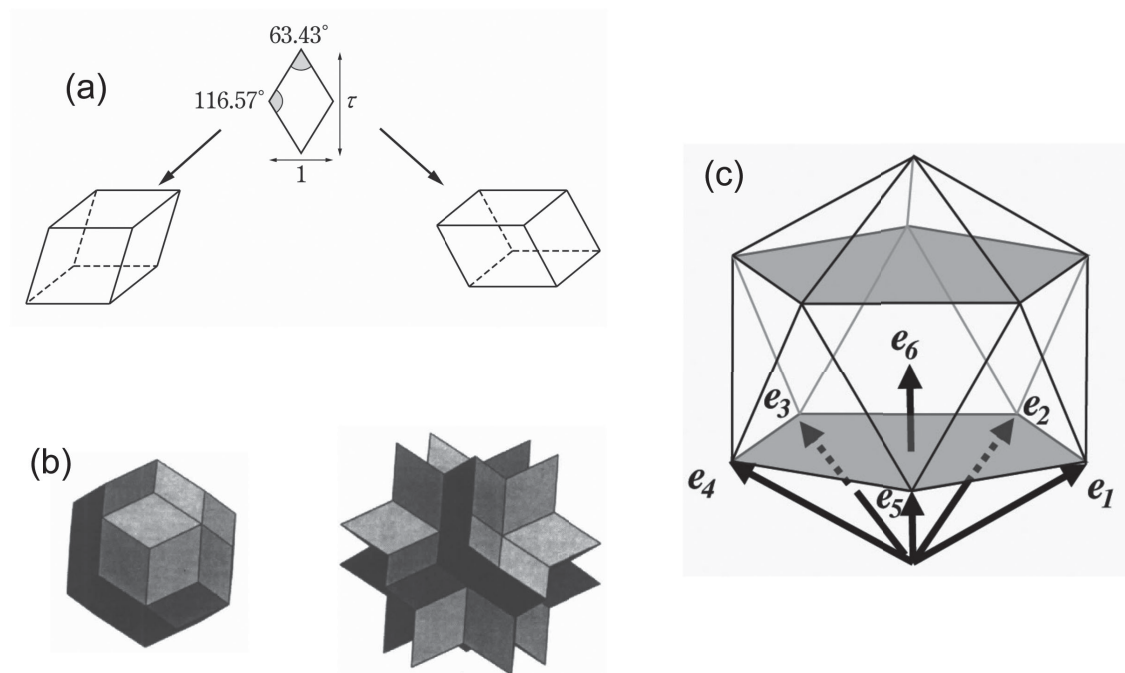


Fig. 7. (a) Acute rhombus (AR) and obtuse rhombus (OR) constructed by a so-called golden rhombus, whose diagonal ratio is  $\tau$ , (b) a rhombic triacontahedron constructed by ten AR and ten OR, and a stellated dodecahedron constructed by twenty AR, (c) six basis vectors used to index lattice of IQC, described by an icosahedron.

bohedra can be packed to form a rhombic triacontahedron (RTH), and twenty acute rhombohedra can be packed to form a stellated dodecahedron. Both polyhedrons reveal an icosahedral symmetry, which gives an image that how the unit cells can be packed to fill space. By using polyhedrons as unit cells with atomic decoration, it is easy to image the symmetry of structure, which also reduces constraints of matching rules.

Similar to the case of Penrose patterns, a three-

dimensional quasi-periodic structure can be obtained by cut-and-projection method of a six-dimensional cubic lattice onto a three-dimensional space. The typical  $W$  (window) for the projection is a rhombic triacontahedron shape with edge length  $1/\tau^2$  times that of projected structure (Henley, 1986). In the six-dimensional construction the analogy of  $W$  in Fig. 4 is a product of a three-plane and a suitable three-dimensional cross section. The  $L$  and  $S$  line segments correspond to acute and obtuse rhombohe-

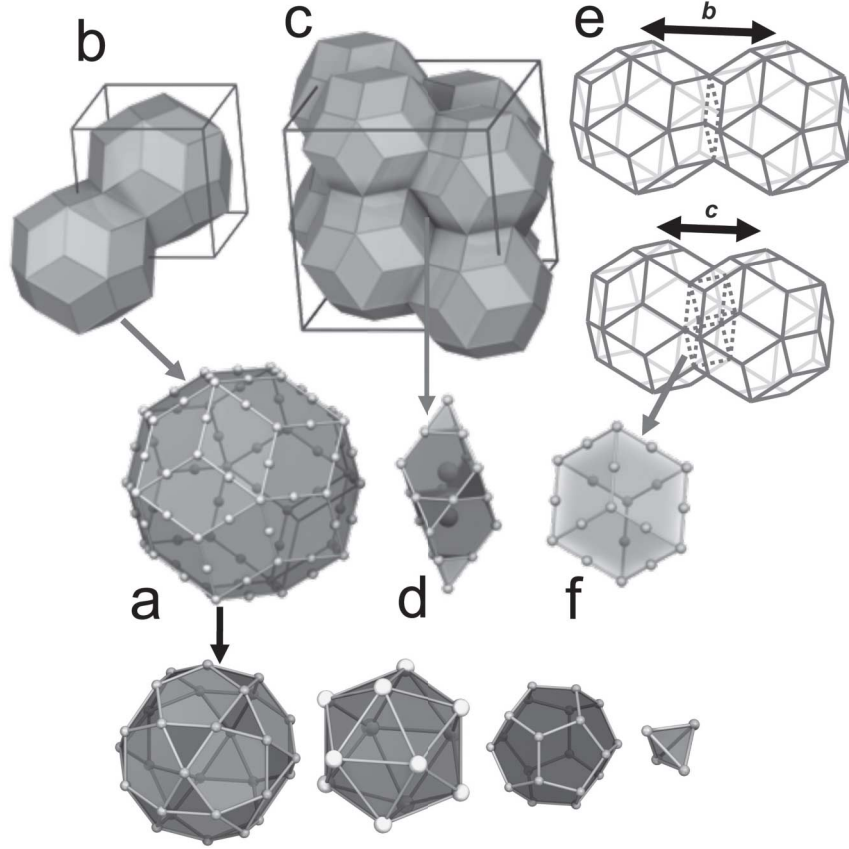


Fig. 8. (a) A rhombic triacontahedral (RTH) unit with atomic decoration used to construct (b) 1/1 and (c) 2/1 approximants in Cd-Yb system, where the structure of 1/1 approximant can be described by the RTH and structure of 2/1 approximant needs (d) Yb and Al decorated AR unit in addition to the RTH. There are only two linkages between two adjacent RTH are allowed: (e) b-linkage link by sharing a rhombus unit and (f) c-linkage connected by overlapping an OR (Takakura *et al.*, 2007).

dra, respectively. If the vectors used to describe  $\mathbf{W}$  are a series of  $(m, 1, 0)$  vectors, then the three-dimensional quasi-periodic structure results when  $m \rightarrow \tau$ . By taking the rational approximants  $m = 0/1, 1/1, 1/2, 2/3 \dots$ , one obtains a sequence of cubic structures with larger and larger lattice constants. Two 1/1 approximants have been verified in  $\alpha$ -AlMnSi (Elser and Henley, 1985) and  $(\text{Al,Zn})_{49}\text{Mg}_{32}$  (Henley and Elser, 1986) compounds, which are bcc packing of icosahedral clusters with different shell structures for two systems. By performing quenching (a rapid cooling), IQCs were formed in these two alloys, hence two compounds are corresponding approximants to two IQCs. For the same of simplicity, it could be said that both IQC and approximant consist of icosahedral clusters, whose arrangement is quasi-periodic for the former and periodic for the later, respectively. Therefore, the approximants contain very useful information in the three-dimensional case for building initial structural model of IQCs. Lattice points of IQC are normally assigned with six vectors expressed on an icosahedron, namely  $e_1, e_2, e_3, e_4, e_5$  and  $e_6$  as shown in Fig. 7(c). A possible basis for the diffraction spots of an IQC is given by the following six vectors (Elser, 1985).

$$a_i^* = \frac{1}{a}(1, \tau, 0), \frac{1}{a}(-1, \tau, 0), \frac{1}{a}(0, 1, \tau), \\ \frac{1}{a}(\tau, 0, 1), \frac{1}{a}(\tau, 0, -1), \frac{1}{a}(0, 1, -\tau) \quad (5)$$

where  $i = 1, \dots, 6$ .

So far, there is only one IQC, namely  $i$ -Cd<sub>5.7</sub>Yb (Tsai *et al.*, 2000), whose structure has been completely solved (Takakura *et al.*, 2007). A cubic phase Cd<sub>6</sub>Yb with a space group of  $Im\bar{3}$  ( $I$ : body centered lattice,  $m$ : reflection plane,  $\bar{3}$ : 3-fold axes with an inversion) and lattice parameter  $a = 0.156$  nm exists in the Cd-Yb phase diagram (Palenzona, 1971). The structure of Cd<sub>6</sub>Yb has been determined and it was demonstrated to be a 1/1 approximant to the IQC phase. A phase Cd<sub>5.7</sub>Yb adjacent to the Cd<sub>6</sub>Yb phase in the phase diagram is an IQC. The shell structure of the icosahedral cluster deduced from Cd<sub>6</sub>Yb is shown in Fig. 8(a), whose structure is explained as follows. The first shell is created by four Cd atoms around the cluster center, the second shell consists of 20 Cd atoms forming a dodecahedron, the third shell is an icosahedron made of 12 Yb atoms, the fourth shell is a Cd icosidodecahedron obtained by placing 30 Cd atoms on the edges of the Yb icosahedron, and the fifth shell is a RTH (rhombic triacontahedron) in which Cd atoms are located on 32 vertices and 60 edge centers. Recently, a detailed structure for  $i$ -Cd<sub>5.7</sub>Yb has been determined by single-grain X-ray diffraction, where the icosahedral cluster, which contains five atomic shells (Fig. 8(a)) and is a RTH cluster, was demonstrated to be identical to that of the Cd<sub>6</sub>Yb approximant. It is important to indicate that each kind of atom occupy definite position in the RTH

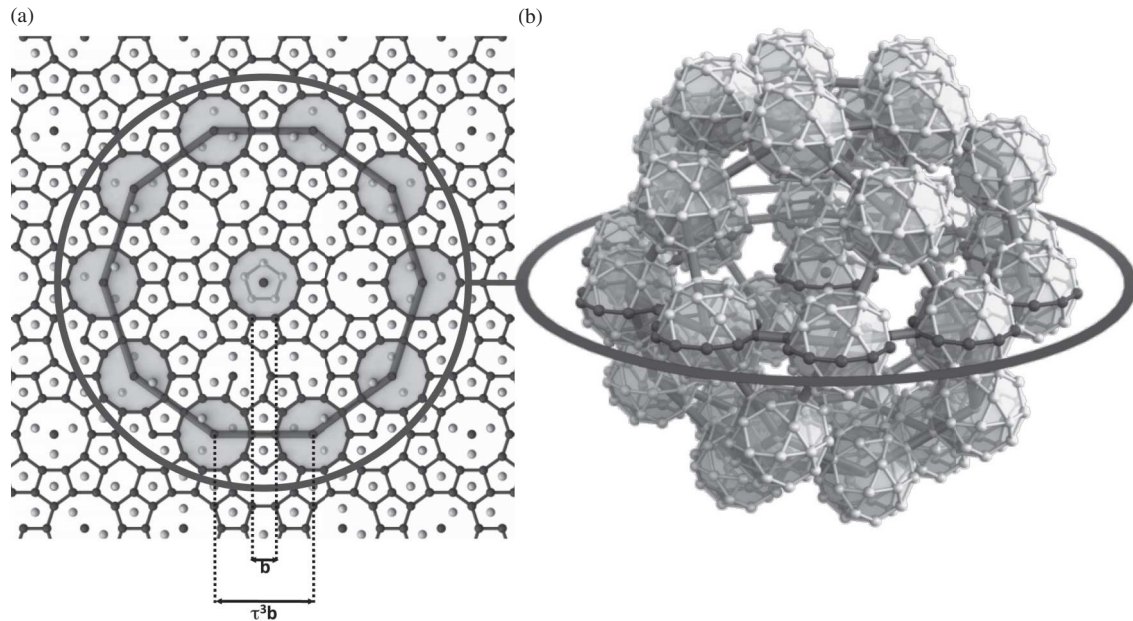


Fig. 9. Structural description of  $i\text{-Cd}_{5.7}\text{Yb}$  with RTH unit. (a) A dense plane of RTH units is seen along a fivefold axis. (b) A small ball represents a RTH unit used to construct an icosidodecahedron cluster, by which a larger icosidodecahedron cluster can be built up. Ratio of edge length between large and small icosidodecahedra is  $\tau^3$  (Takakura *et al.*, 2007).

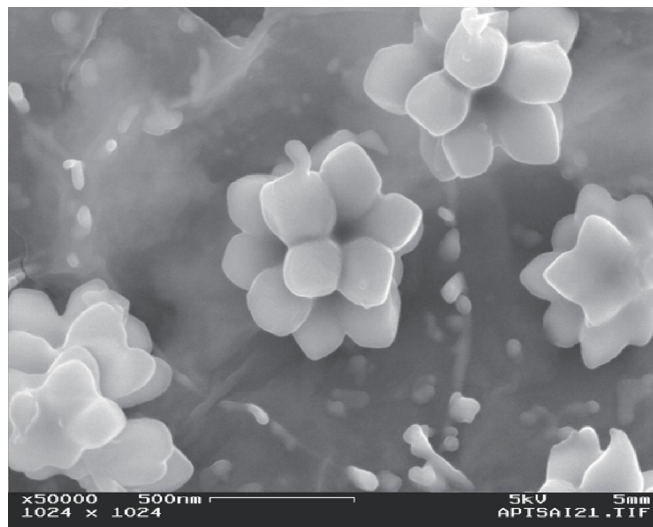


Fig. 10. A SEM image of melt-quenched  $\text{A}_{94}\text{Mn}_6$  alloy after etching treatment. IQC reveals a stellated dodecahedral form.

cluster, where Yb (only on icosahedral shell) and Cd occupy different atomic sites. This is a great advantage for structural analysis.

The structure of 1/1 approximant is a bcc packing of RTH clusters as shown in Fig. 8(b). Furthermore, structure of a 2/1 approximant (Fig. 8(c)) was solved to consist of the same RTH as 1/1 approximant but it needs an additional unit (Gómez and Lidin, 2001), namely, an acute rhombohedron (Fig. 8(d)) with suitable atomic decoration to fill the cavity. In both approximants the RTH clusters are linked to each other (Fig. 8(e)) along two-fold (**b**-bond) directions by sharing a rhombus face and three-fold direction (**c**-bond) with interpenetration of an obtuse rhombohedron as shown in Fig. 8(f). Consequently, three fundamen-

tal building units: a RTH cluster (a), an acute (d) and an obtuse rhombohedron (f) are supposed to be necessary for constructing the IQC structure.

Combined with knowledge of linkage rules and building units, a precise structural model for Cd-Yb IQC ( $i\text{-Cd-Yb}$ ) was proposed as shown in Fig. 9, which describes the structure of  $i\text{-Cd-Yb}$  in terms of inflation and hierarchical packing of clusters. Here, the term “inflation” means the property that a subset of special points from the original structure has an arrangement identical to the original one when the subset is increased in scale by a particular scale, which is  $\tau^3$  in this case. Figure 9 shows the RTH center positions (grey circles) and their connection on a plane with five-fold symmetry. Starting from the center, it can be shown that a

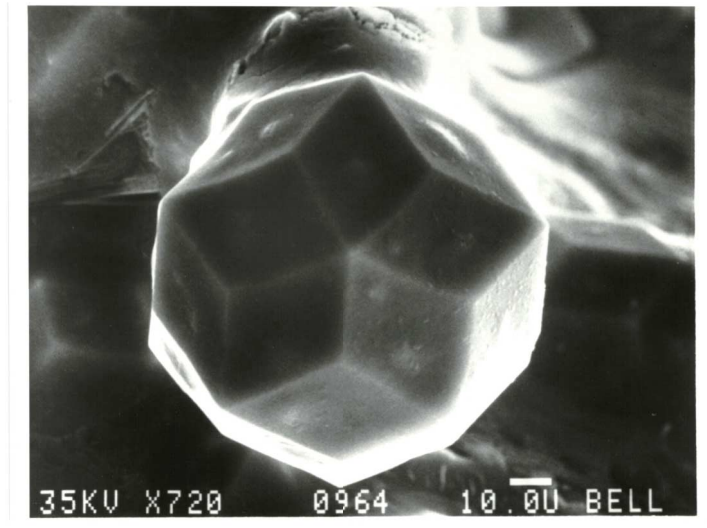


Fig. 11. A SEM image for an isolated single IQC with a rhombic triacontahedral morphology in Al-Li-Cu alloy (Kortan *et al.*, 1989).

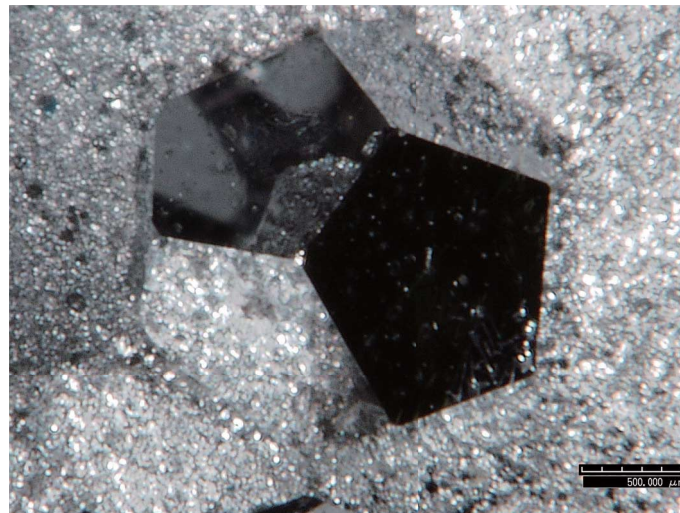


Fig. 12. A Single grain of Zn-Mg-Dy IQC prepared by solution growth process.

cluster of RTH units (icosidodecahedron) is formed. The cluster of RTH is at the center of a large “cluster of cluster”, which is also icosidodecahedron but  $\tau^3$  times increase in scale. A prominent feature of the model is that almost all the IQC structure is described in terms of interpenetrating RTH clusters, where 93.8% of the atoms belong to the RTH clusters (Takakura *et al.*, 2007). On the other hand, full structure of the 1/1 approximant is described by the RTH clusters, where 100% of atoms belong to the RTH clusters. These two structures both described by the RTH clusters but standing at two opposing extremes, have a difference in composition only by about 2 at.% (atomic %), and a difference in atomic decoration by about 6% of atoms. In the aspect of cluster formation, structures of IQC and approximants seem to be understood in a simple manner. One interesting feature is that all approximants exist as stable phases in nature, which can be mathematically derived by cut and projection scheme.

### 3. Morphologies of Quasicrystals

The complete structural solution of *i*-Cd-Yb, is helpful for understanding growth mechanism of QCs. Studies on surface structure of QCs also provided a lot of crucial information for understanding growth morphology and stability. Indeed, understanding stability and morphologies of QCs surfaces is intimately related to getting insight into growth process of QCs.

#### 3.1 Stellated polyhedron

In most of early experiments, QCs synthesized by rapid solidification revealed highly dendritic morphologies. In short, visible pentagon dodecahedra around 0.01 mm in size were observed in melt-quenched AlMnSi (Csanady *et al.*, 1990). For alloys containing lower contents of Mn (below 8 at.%), a stellated polyhedron as shown in Fig. 10 showed up. This resembles to one of polyhedron in three-dimensional quasi-periodic lattice as shown in Fig. 7(b), which is composed of twenty acute rhombohedra and ex-

hibits icosahedral symmetry. These beautiful stellated polyhedral morphologies are only observed in low-Mn-contents Al alloys, because formation of a small number of nuclei in the melt upon solidification which allowed equiaxial growth of IQC grains. In view of morphologies, it seems that preferential growth direction is oriented to the three-fold direction.

### 3.2 Rhombic triacontahedron

One of most beautiful morphologies was observed in conventional solidification state of *i*-Al-Li-Cu ( $\text{Al}_{5.5}\text{Li}_3\text{Cu}$ ), which exhibits a form of rhombic triacontahedron (Dubost *et al.*, 1986; Kortan *et al.*, 1989) as shown in Fig. 11. This is another polyhedron existing in three-dimensional quasi-periodic lattice, which is consisted of ten acute rhombohedra and ten obtuse rhombohedra. Since this IQC is unstable in air due to the selected oxidation of Li, very few detailed investigations were done.

### 3.3 Pentagonal dodecahedron

This is the morphology most often observed in IQCs. As mentioned previously, distorted dodecahedral grains of about 0.01 mm were observed in melt-quenched Al-Mn alloys. Later, clear morphologies were observed in conventionally solidified Al-Cu-Fe and Ga-Mg-Zn alloys. The similar morphologies with grain sizes of about 1 mm were also observed in most stable IQCs such as *i*-Al-Cu-Ru, *i*-Al-Pd-Re, *i*-Zn-Mg-RE and *i*-Ag-In-Yb. As mentioned previously, all stable IQCs, except *i*-Cd-Yb and *i*-Ag-In-Yb, form through reactions between a liquid and a intermetallic phases upon solidification. Object shown in Fig. 12 is a single grain of Zn-Mg-Dy IQC with perfect pentagonal dodecahedral morphology grown by the solution growth method. Recently, single grains grown by this process could acquire sizes of 2~10 mm. According to the their morphologies, it is clear that the IQCs in this case are not dendritic growth. Instead, observation of larger and flat pentagonal planes indicates planar growth of IQCs along six five-fold axes in slow cooling.

Surface studies on the *i*-Ag-In-Yb and *i*-Al-Pd-Mn showed that five-fold planes have a flat structure, which is exact enough for obtaining atomic resolution (Sharma *et al.*, 2007). This is an evidence that the five-fold planes are rel-

atively stable, which have terminated at planes containing relatively high concentrations of Yb (40 at.%) for *i*-Ag-In-Yb (16 at.% Yb) and of Al (~80 at.%) for *i*-Al-Pd-Mn (70 at.% Al), compared to their bulk compositions. According to structure models, atomic densities  $\rho$  are highest on two-fold planes ( $\rho_2 > \rho_5 > \rho_3$ ) in these two IQCs. Namely, Yb and Al with relatively low surface energies (Vitos *et al.*, 1998) with respect to the rest two constituent elements have concentrated at five-fold planes owing to their sufficiently lower surface energy. Especially, during the crystal growth produced by solution growth process, the lower surface energies of Yb and Al would reduce solid-liquid interfacial energies, and consequently the pentagonal dodecahedron with five-fold surfaces are formed. Finally, it would be interesting to note that the surface preparation contains valuable information of morphology of IQCs.

### References

- Csanady, A., Rapp, K., Dobosy, M. and Bauer, M. (1990) *Symmetry*, **1**, 75.  
 de Bruijn, N. G. (1981) *Proc. Kon. Ned. Akad. Wetenschap.*, **A84**, 39.  
 Dubost, B., Lang, J. M., Tanaka, M., Sainfort, P. and Audier, M. (1986) *Nature*, **324**, 48.  
 Elser, V. (1985) *Phys. Rev.*, **B32**, 4892.  
 Elser, V. and Henley, C. L. (1985) *Phys. Rev. Lett.*, **55**, 2883.  
 Gómez, C. P. and Lidin, S. (2001) *Angew. Chem. Int. Ed.*, **40**, 4037.  
 Henley, C. L. (1986) *Phys. Rev.*, **B34**, 797.  
 Henley, C. L. and Elser, V. (1986) *Phil. Mag.*, **B53**, 59.  
 International Union of Crystallography (1992) *Acta. Cryst.*, **A48**, 922.  
 Kortan, A. R., Chen, H. S., Parsey, J. M., Jr. and Kimerling, L. C. (1989) *J. Mater. Sci.*, **24**, 1999.  
 Palenzona, A. (1971) *J. Less-Common Met.*, **25**, 367.  
 Sharma, H. R., Shimoda, M. and Tsai, A. P. (2007) *Adv. Phys.*, **56**, 403.  
 Shechtman, D., Blech, I., Gratias, D. and Cahn, J. W. (1984) *Phys. Rev. Lett.*, **53**, 1951.  
 Takakura, H., Gomez, C. P., Yamamoto, A., deBoissieu, M. and Tsai, A. P. (2007) *Nature Materials*, **6**, 58.  
 Tsai, A. P. (1999) *Physical Properties of Quasicrystal* (ed. Z. Stadnik), *Springer Series in Solid-State Science*, 126, Springer-Verlag, Berlin, Heidelberg, p. 5.  
 Tsai, A. P. (2013) *Chem. Soc. Rev.*, **42**, 5352.  
 Tsai, A. P. and Cui, C. (2015) Crystal growth of quasicrystals, in *Handbook of Crystal Growth*, Vol. I (ed. T. Nishinaga), pp. 1113–1156, Elsevier.  
 Tsai, A. P., Guo, J. Q., Abe, E., Takakura, H. and Sato, T. J. (2000) *Nature*, **408**, 537.  
 Vitos, L., Ruban, A. V., Skriver, H. L. and Kollar, J. (1998) *Surf. Sci.*, **411**, 186.  
 Yamamoto, A. (1996) *Acta Crystal.*, **A52**, 509.